Human Molecular Genetics, 2011, Vol. 20, No. 24 **4978–4990**
doi:10.1093/hmg/ddr433
Advance Access published on September 23, 2011

Expression of the dystrophin isoform Dp116 preserves functional muscle mass and extends lifespan without preventing dystrophy in severely dystrophic mice

Luke M. Judge[1,2,3], Andrea L.H. Arnett[1,2,3], Glen B. Banks[1] and Jeffrey S. Chamberlain[1,4,5,*]

[1]Department of Neurology, [2]Program in Molecular and Cellular Biology, [3]The Medical Scientist Training Program, [4]Department of Medicine and [5]Department of Biochemistry, University of Washington, 1959 NE Pacific St, Seattle, WA 98195-7720, USA

Received July 23, 2011; Revised September 9, 2011; Accepted September 19, 2011

Dp116 is a non-muscle isoform of dystrophin that assembles the dystrophin–glycoprotein complex (DGC), but lacks actin-binding domains. To examine the functional role of the DGC, we expressed the Dp116 transgene in mice lacking both dystrophin and utrophin (*mdx:utrn*$^{-/-}$). Unexpectedly, expression of Dp116 prevented the most severe aspects of the *mdx:utrn*$^{-/-}$ phenotype. *Dp116:mdx:utrn*$^{-/-}$ transgenic mice had dramatic improvements in growth, mobility and lifespan compared with controls. This was associated with increased muscle mass and force generating capacity of limb muscles, although myofiber size and specific force were unchanged. Conversely, Dp116 had no effect on dystrophic injury as determined by muscle histopathology and serum creatine kinase levels. Dp116 also failed to restore normal fiber-type distribution or the post-synaptic architecture of the neuromuscular junction. These data demonstrate that the DGC is critical for growth and maintenance of muscle mass, a function that is independent of the ability to prevent dystrophic pathophysiology. Likewise, this is the first demonstration in skeletal muscle of a positive functional role for a dystrophin protein that lacks actin-binding domains. We conclude that both mechanical and non-mechanical functions of dystrophin are important for its role in skeletal muscle.

INTRODUCTION

Duchenne muscular dystrophy (DMD) is a severe muscle-wasting disorder caused by mutations in the X-chromosome-linked dystrophin gene. The disease is relatively common, affecting 1 in 3500 males, and has no effective treatment (1). A wide variety of studies of disease pathogenesis have been performed using the *mdx* mouse model, a naturally occurring dystrophin-deficient strain (2). Muscles in *mdx* mice show many of the histological characteristics of early DMD muscles, including necrosis, inflammation and regenerating myofibers (3,4). Despite being an exact genetic model of DMD, the *mdx* mouse has been criticized for a failure to recapitulate the severe progressive nature of muscular dystrophy in humans (5). Unlike humans, *mdx* mice do not have a dramatically shortened lifespan, and display muscle hypertrophy and retention of muscle function throughout the majority of their life (6–8). In contrast, mice deficient in both dystrophin and its autosomal homologue utrophin (*mdx:utrn*$^{-/-}$) display many of the severe features of DMD, including growth retardation, skeletal deformities and premature death (9,10). This observation supports the hypothesis that the upregulation of utrophin observed in *mdx* muscles compensates for dystrophin deficiency, leading to the mild phenotype of these mice. Overexpression of utrophin prevents muscular dystrophy in transgenic *mdx* mice, indicating that utrophin and dystrophin can be functionally redundant (11).

Dystrophin is required for complete assembly of the dystrophin–glycoprotein complex (DGC), which consists of the dystroglycan, sarcoglycan–sarcospan and dystrobrevin–syntrophin sub-complexes (reviewed in 12). Dystrophin interacts with costameric F-actin via its N-terminal and central

*To whom correspondence should be addressed at: Department of Neurology, University of Washington School of Medicine, Box 357720, Seattle, WA 98195-7720, USA. Tel: +1 2062215363; Fax: +1 2066168272; Email: jsc5@uw.edu

actin-binding domains and with transmembrane dystroglycan via its WW and cysteine-rich domains, creating a mechanically strong link between the extracellular matrix and the cytoskeleton (13,14). This link functions to dissipate the forces of contraction from within muscle fibers to the extracellular matrix, protecting the sarcolemma from stresses during exercise, and is referred to as the mechanical function of dystrophin (15,16).

Dystrophin also potentially serves as a scaffold for signaling complexes, as many of the proteins in the DGC bind to or are substrates for known signaling molecules, including neuronal nitric oxide synthase (nNOS), caveolin-3, Grb2 and various kinases (17–22). However, restoration of the DGC without restoring the mechanical function of dystrophin does not improve the phenotype of *mdx* mice (23–25). These results support the hypothesis that the loss of the mechanical function of dystrophin is the primary cause of muscular dystrophy in *mdx* mice. The increased severity of *mdx:utrn*$^{-/-}$ phenotype compared with *mdx* has been largely unexplained, but could be due to further weakening of the mechanical connection between the cytoskeleton and the extracellular matrix, caused by the additional loss of utrophin. Another possible explanation is that utrophin upregulation in *mdx* muscles is adequate for the maintenance of signaling through the DGC, thus the severe consequences of the double mutant are due to the loss of both the mechanical and signaling functions in muscle.

In a previous study, we described transgenic mice that express the dystrophin isoform Dp116 in skeletal muscle (25). Dp116 is normally expressed in Schwann cells of the peripheral nervous system where it associates with a DGC-like complex that, as in skeletal muscle, binds to laminin-2 in the extracellular matrix (26). Furthermore, Dp116 contains the complete dystroglycan-binding domain of dystrophin, but does not have any of the actin-binding motifs, allowing us to dissect the mechanical and signaling properties of dystrophin. Expression of Dp116 and restoration of the DGC did not improve the phenotype of *mdx*^{4cv} mice, consistent with previous studies demonstrating that actin-binding domains of dystrophin are required to prevent dystrophic injury. However, we hypothesized that expression of Dp116 in *mdx:utrn*$^{-/-}$ mice would allow a clearer dissection of the signaling and mechanical roles of dystrophin, as residual utrophin in *mdx* muscle may maintain critical signaling processes. Here we showed that the increased severity of the *mdx:utrn*$^{-/-}$ phenotype compared with that of *mdx* mice is not simply due to a further loss of the structural link between the actin cytoskeleton and the extracellular matrix. Instead, our data suggest that the dystrophin/utrophin glycoprotein complex itself plays an important role in maintaining muscle mass, even in the absence of a mechanically strong link to the cytoskeleton.

RESULTS

Generation of transgenic Dp116 mice on the *mdx:utrn*$^{-/-}$ background

Dp116/mdx transgenic mice were crossed with *mdx:utrn*$^{-/+}$ mice (9) for two generations to obtain *Dp116:mdx:utrn*$^{-/-}$ mice (see Materials and Methods). From nearly 300 pups in line 2197, we obtained 10.9% of the genotype *mdx:utrn*$^{-/-}$ and 7.4% of the genotype *Dp116:mdx:utrn*$^{-/-}$, close to the expected ratio of 12.5% for each genotype. To verify that the genotypes accurately reflected expression of the three gene products of interest, we performed immunofluorescence staining of skeletal muscles using polyclonal antibodies against the dystrophin N-terminus, utrophin-A and the Flag epitope (Fig. 1). Dp116 was appropriately expressed and localized to the sarcolemma in esophagus, diaphragm, intercostal and various hindlimb muscles, although expression in the diaphragm was consistently much lower than in the limb muscles (data not shown). As expected, no significant expression was seen in cardiac muscle because we used the human α-skeletal actin promoter that selectively expresses the transgene in skeletal muscle. We have previously shown that expression of Dp116 at the sarcolemma is sufficient for restoration of the DGC, excluding neuronal nNOS (25).

Dp116 expression increases muscle mass and lifespan of *mdx:utrn*$^{-/-}$ mice

As expected, *mdx:utrn*$^{-/-}$ mice were smaller than their littermates at weaning and showed significant growth retardation throughout their lifespan. Although *Dp116:mdx:utrn*$^{-/-}$ mice were slightly smaller on average than control *Dp116* transgenic mice with a functional utrophin gene (*Dp116:mdx:utrn*$^{-/+}$), they continued to gain body mass at a similar rate until beyond 20 weeks of age (Fig. 2A). Control *mdx:utrn*$^{-/-}$ mice developed severe kyphosis of the spine, joint contractures and reduced mobility between 8 and 10 weeks of age. In contrast, *Dp116:mdx:utrn*$^{-/-}$ mice did not develop any of these overt signs of muscle weakness and were essentially indistinguishable from their littermates that expressed utrophin (Fig. 2C and Supplementary Material, Movie). Consistent with their improved physical appearance, *Dp116:mdx:utrn*$^{-/-}$ mice had a longer lifespan than the non-transgenic controls (Fig. 2B). The median lifespan of *mdx:utrn*$^{-/-}$ mice in this study was 12 weeks ($n = 21$, 7 males, 14 females) with the longest lived mouse reaching 20 weeks of age. In contrast, the median lifespan of *Dp116:mdx:utrn*$^{-/-}$ transgenic animals from line 2197 ($n = 15$, 10 males, 5 females) was found to be 46 weeks. Interestingly, none of the female mice lived beyond 46 weeks of age, while 7 of the 10 male mice lived beyond 46 weeks of age. To confirm that the effect was specific to the *Dp116* transgene, we crossed the independent line 2354 onto the *mdx:utrn*$^{-/-}$ background. Thus far several mice from this line (including both males and females) have surpassed 35 weeks of age and have shown similar growth, weight gain and mobility compared with line 2197. We also observed *Dp116:mdx:utrn*$^{+/-}$ mice as controls ($n = 7$, all males). One of these mice developed a tumor and had to be euthanized at 42 weeks age, but the remaining 6 have remained healthy for greater than 1 year.

We sacrificed C57Bl/6, *mdx*, *mdx:utrn*$^{-/-}$ and *Dp116:mdx:utrn*$^{-/-}$ mice at 8 weeks of age to examine their skeletal muscles. The mass of both the tibialis anterior (TA) and quadriceps muscles was increased in *Dp116:mdx:utrn*$^{-/-}$ mice relative to *mdx:utrn*$^{-/-}$ controls, although not to the extent of corresponding *mdx* muscles (Table 1). The total

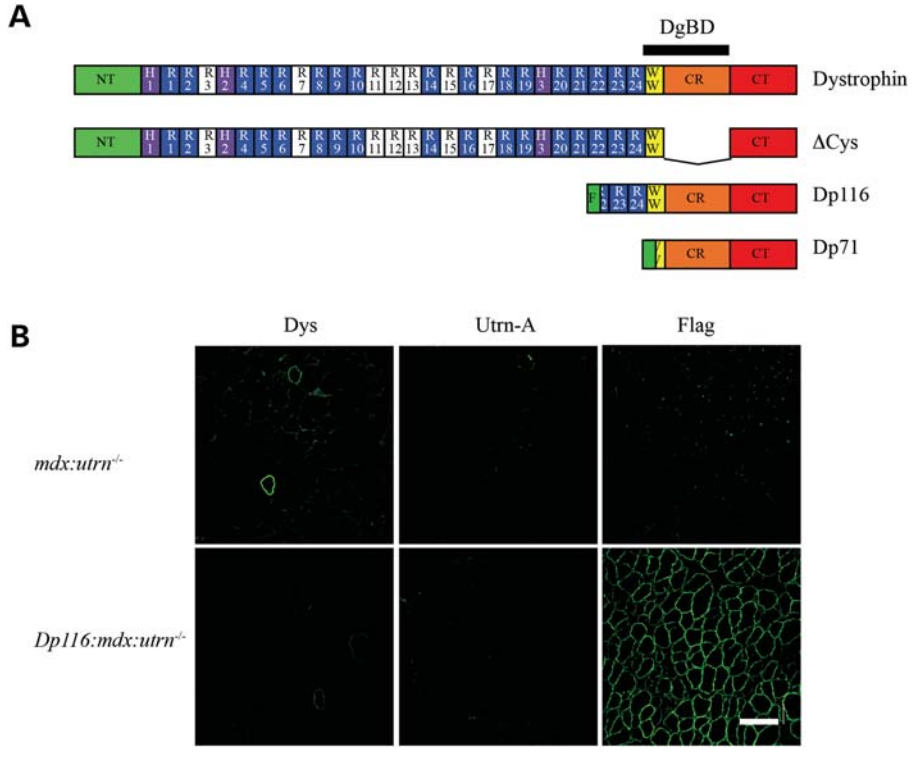

Figure 1. Expression of dystrophin, utrophin and Dp116 in transgenic mice. (**A**) Domain structure of dystrophin and selected isoforms tested as transgenes in *mdx:utrn*$^{-/-}$ mice. NT, NH_2-terminal actin-binding domain; H , hinge; R, spectrin-like repeat; W, WW domain; CR, cysteine-rich domain; CT, carboxy-terminal domain, DgBD, dystroglycan-binding domain; F, Flag epitope tag. Both Dp71 and Dp116 have unique NH_2-terminal peptides, shown in green. The Dp116 protein expressed in this study has a Flag epitope tag incorporated upstream of the unique peptide. Basic spectrin-like repeats that contribute to the central rod actin-binding domain are shown in white. (**B**) Immunofluorescent staining of quadriceps muscles for full-length dystrophin, utrophin-A and Dp116. Dystrophin (Dys) is only detected in rare, revertant myofibers in *mdx:utrn*$^{-/-}$ mice. Utrophin-A (Utrn-A) is not detected in any of the mice analyzed. Flag epitope-tagged Dp116 is localized to the sarcolemma in transgenic *Dp116:mdx:utrn*$^{-/-}$ myofibers. Scale bar: 100 μm.

cross-sectional area of hematoxylin and eosin-stained sections of *Dp116:mdx:utrn*$^{-/-}$ muscles was increased compared with the *mdx:utrn*$^{-/-}$ controls but not compared with *mdx*, consistent with the increase in total muscle mass (Fig. 3A). Serum creatine kinase levels were also measured for wild-type, *mdx:utrn*$^{-/-}$ and *Dp116:mdx:utrn*$^{-/-}$ mice. Both *mdx:utrn*$^{-/-}$ and *Dp116:mdx:utrn*$^{-/-}$ mice had serum creatine kinase levels ∼10-fold higher than wild-type controls but did not differ significantly from each other (Table 1).

Dp116 expression does not improve histopathology or mechanical properties of *mdx:utrn*$^{-/-}$ muscles

Examination of hematoxylin and eosin-stained cross-sections showed no gross improvement in dystrophic pathology in quadriceps muscles from *Dp116:mdx:utrn*$^{-/-}$ mice compared with *mdx or mdx:utrn*$^{-/-}$ muscles (Fig. 3). Similar pathology was found in the TA, soleus, diaphragm and intercostal muscles (data not shown). These results indicate that although muscle mass and function is preserved in *Dp116:mdx:utrn*$^{-/-}$ mice, this cannot be explained by protection from dystrophic damage. Myofiber cross-sectional area was reduced to a similar extent (median cross-sectional area 37% of wild-type) in both *Dp116:mdx:utrn*$^{-/-}$ and *mdx:utrn*$^{-/-}$ mice and the percentage of centrally nucleated fibers remained elevated at >70% (Fig. 4A and C). The density of myofibers was measured independently to determine whether the increase in total muscle mass seen in *Dp116:mdx:utrn*$^{-/-}$ was due to accumulation of non-muscle tissue or an increase in absolute number of muscle fibers. Fiber density was similar in both *Dp116:mdx:utrn*$^{-/-}$ mice and *mdx:utrn*$^{-/-}$ (Fig. 4B), indicating that fibrosis and the accumulation of other non-muscle tissues are not responsible for the observed increase in gross muscle mass.

Muscles from *mdx* and *mdx:utrn*$^{-/-}$ mice display increased susceptibility to contraction-induced injury and a reduction in specific force (27,28). We evaluated mechanical properties of the TA in *Dp116:mdx:utrn*$^{-/-}$ mice and compared this to both *mdx* and *mdx:utrn*$^{-/-}$ to determine whether there was any improvement in the transgenic animals. Maximal force generation at optimal fiber length was increased by ∼50% in *Dp116:mdx:utrn*$^{-/-}$ animals when compared with *mdx:utrn*$^{-/-}$ mice, confirming that the increased gross muscle mass in the *Dp116:mdx:utrn*$^{-/-}$ mice is largely composed of functional muscle tissue (Fig. 4D). However, specific force (force/cross-sectional area) was not significantly improved (Fig. 4E). Interestingly, *Dp116:mdx:utrn*$^{-/-}$ mice demonstrated an improved resistance to contraction-induced injury that was similar to that seen in *mdx* mice, but remained reduced when compared with C57Bl/6 controls (Fig. 4F).

An established characteristic of *mdx:utrn*$^{-/-}$ muscles is a preponderance of oxidative muscle fibers and upregulation

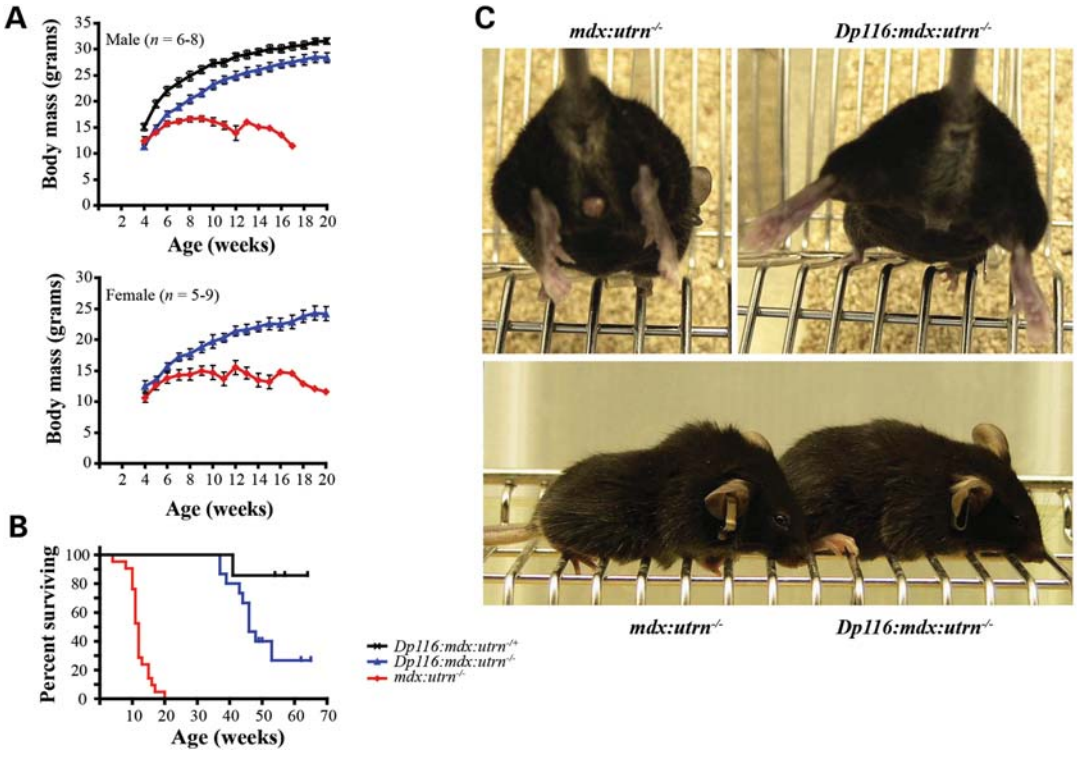

Figure 2. Expression of Dp116 increases viability of *mdx:utrn*$^{-/-}$ mice. (**A**) Both male and female transgenic *Dp116:mdx:utrn*$^{-/-}$ mice had continued weight gain after 10 weeks of age, while the control *mdx:utrn*$^{-/-}$ mice displayed a failure to thrive beyond 10 weeks of age. However, the transgenic *Dp116:mdx:utrn*$^{-/-}$ mice were consistently smaller than transgenic mice with one functional utrophin allele. Error bars signify $\pm$SEM and are not shown for time points where only one surviving mouse remained in the cohort. (**B**) Expression of Dp116 increased lifespan of *mdx:utrn*$^{-/-}$ mice. Kaplan–Meier analysis demonstrated a significant increase in survival ($P < 0.0001$) of *Dp116:mdx:utrn*$^{-/-}$ mice ($n = 15$, 5 females, 10 males) compared with control *mdx:utrn*$^{-/-}$ mice ($n = 21$, 14 females, 7 males). Each tick-mark in the transgenic cohort indicates the age of a surviving mouse at the end of this study. (**C**) An 11-week-old *mdx:utrn*$^{-/-}$ male is shown to demonstrate joint contractures of the hind limbs (upper left). The *Dp116:mdx:utrn*$^{-/-}$ male littermate does not suffer from joint contractures and is able to extend its hind limbs (upper right). The same littermates are shown in the lower panel to demonstrate that spinal kyphosis and reduced musculature in the *mdx:utrn*$^{-/-}$ control (*left*) are absent in the *Dp116* transgenic littermate (right).

Table 1. Comparison of muscle mass and serum creatine kinase levels in age-matched transgenic and control mice

	C57Bl/6	*mdx*	*mdx:utrn*$^{-/-}$	*Dp116:mdx:utrn*$^{-/-}$
TA mass (mg)	36.7 $\pm$ 2.0	65.9 $\pm$ 1.6*	31.9 $\pm$ 2.6	41.1 $\pm$ 0.90***
Quad mass (mg)	165.2 $\pm$ 1.5*	233.7 $\pm$ 3.2*	132.0 $\pm$ 7.4	158.5 $\pm$ 4.5**
Serum CK (U/L)	670 $\pm$ 149***	ND	8473 $\pm$ 2780	6575 $\pm$ 1350

Significantly different from *mdx:utrn*$^{-/-}$: *$P < 0.001$, **$P < 0.01$, ***$P < 0.05$.

of slow muscle genes, which has been proposed to reflect a signaling defect that could contribute to the severe phenotype of these mice (29,30). We performed nicotinamide adenine dinucleotide (NADH) staining on sections of quadriceps and TA muscles from wild-type, *mdx*, *mdx:utrn*$^{-/-}$ and *Dp116:mdx:utrn*$^{-/-}$ mice to determine the oxidative potential of myofibers. Wild-type TA and quadriceps muscles showed a mosaic pattern of darkly stained oxidative and lightly stained glycolytic fibers (Fig. 5). Conversely, both *Dp116:mdx:utrn*$^{-/-}$ and *mdx:utrn*$^{-/-}$ muscles had more dark and intermediate staining showing an increased population of oxidative fibers (Fig. 5). These data show that the abnormal fiber-type distribution seen in *mdx:utrn*$^{-/-}$ muscles is correlated with the severe dystrophy in these mice, but is not sufficient to cause the failure to thrive and dysfunction associated with the phenotype.

Esophageal pathology may contribute to mortality in *Dp116:mdx:utrn*$^{-/-}$ mice

Despite a dramatic increase in longevity and muscle mass in *Dp116:mdx:utrn*$^{-/-}$ mice, average lifespan remained reduced compared with control animals (Fig. 2B). Mice remained active and healthy for several months, but their condition began to deteriorate ~2 weeks before death. The exact cause of death in these mice is unclear; however, we have repeatedly observed a grossly dilated esophagus in aged mice examined post-mortem (Supplementary Material, Fig. S1). This esophageal pathology correlated with lethargic behavior, a reduction in total body mass, and disheveled appearance prior to death (Supplementary Material, Fig. S1C). The end-stage esophagus was severely dilated compared with esophagi isolated from

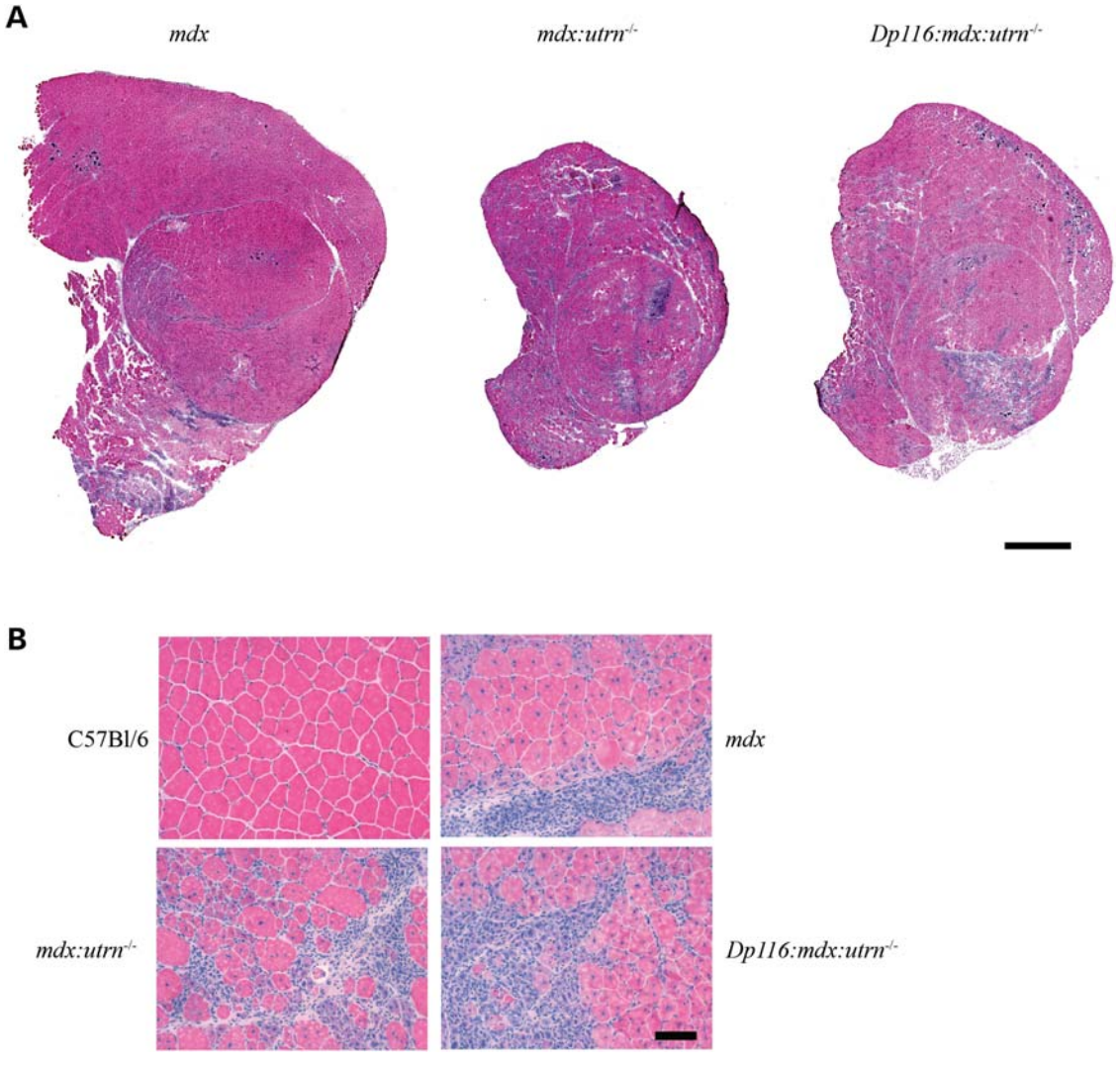

Figure 3. Histology of quadriceps muscles from 8-week-old transgenic and control mice. (**A**) Entire cross-sections from the mid-belly of quadriceps muscles indicate extensive degeneration in both *mdx:utrn*$^{-/-}$ and transgenic *Dp116:mdx:utrn*$^{-/-}$ muscles compared with *mdx*. Scale bar: 1 mm. (**B**) High power (20×) fields of the muscles shown above along with wild-type control. Pathology of *mdx* and *mdx:utrn*$^{-/-}$ skeletal muscles is qualitatively similar at this age, with areas of extensive necrosis, inflammatory infiltrate and large numbers of myofiber containing centrally located nuclei. Similar pathologic changes are seen in the *Dp116* transgenic muscles. Scale bar: 50 μm.

8-week-old animals, indicating that gross esophageal deformities developed with age and were not present from birth in *Dp116:mdx:utrn*$^{-/-}$ mice. Dilation was most pronounced in the region of the esophagus located immediately adjacent to the diaphragmatic esophageal hiatus, above the rostral surface of the diaphragm. In addition, esophagi in aged animals were found to be impacted with solid food, bedding debris and hair (Supplementary Material, Fig. S1A). A similar pathology was not observed in terminal *mdx:utrn*$^{-/-}$ mice, nor was any similar pathology observed in *Dp116:mdx:utrn*$^{-/-}$ mice at 8 or 12 weeks of age (Fig. 6A, Supplementary Material, Fig. S1A and data not shown).

Closer inspection of esophageal cross-sections revealed morphological changes in the esophageal walls (Fig. 6A). Both the mucosal epithelium and the muscularis externa were remarkably reduced in overall thickness. In addition, qualitative changes were apparent within the individual layers of the mucosal epithelium. The cornified epithelium was hyperkeratinized, which may represent a reactive response to abrasion, secondary to impaired transport of solid foods through the esophagus. In contrast, intermediate epithelial zones were significantly reduced or absent. The causative factors leading to esophageal impaction and dilation remain to be deciphered, but may be related to impaired esophageal motility, incomplete mastication of solid food or diaphragmatic stricture. It is important to note that the human α-skeletal actin promoter directs Dp116 expression in skeletal muscle throughout the length of the esophagus (Fig. 6B), and thus, esophageal pathology cannot be attributed to loss of DGC expression in skeletal muscle.

Dp116:mdx:utrn$^{-/-}$ mice display fragmented neuromuscular junctions

The DGC also functions to promote the maturation and maintenance of the neuromuscular synapse (31,32). The neuromuscular

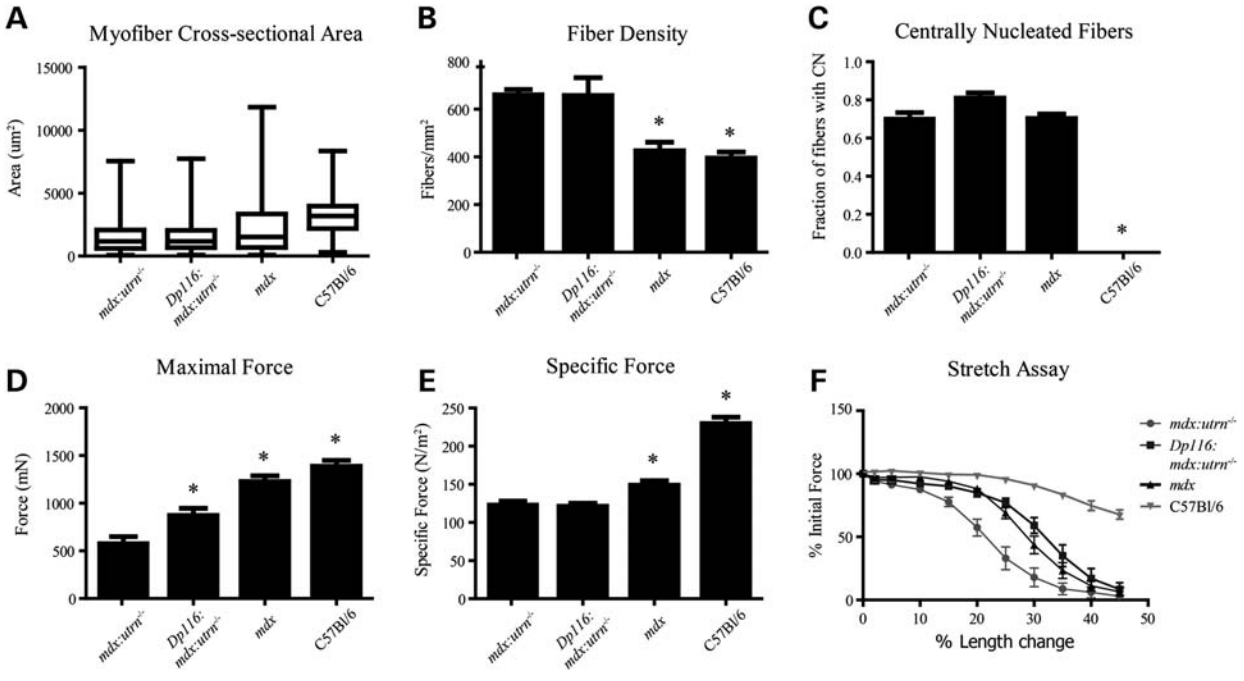

Figure 4. Evaluation of myofibers and contractile properties of TA in *Dp116:mdx:utrn*$^{-/-}$ mice. (**A**) Myofiber cross-sectional area ($n = 500$ fibers per animal) and (**B**) density ($n =$ four 0.13 mm^2 fields per muscle) are unaffected by Dp116 expression and remain reduced compared with age-matched C57Bl/6 and *mdx* animals. (**C**) The percentage of myofibers with centrally located nuclei ($n =$ four 0.13 mm^2 fields per muscle) was not significantly different from that shown in *mdx* or *mdx:utrn*$^{-/-}$ animals. (**D**) Maximal force is increased in *Dp116:mdx:utrn*$^{-/-}$ mice when compared with *mdx:utrn*$^{-/-}$ mice, but (**E**) specific force remains low. (**F**) Contractile performance after lengthening contractions with progressively increasing strain is improved in *Dp116:mdx:utrn*$^{-/-}$ mice, but is still reduced below that shown in wild-type animals; $n = 5–7$ animals per group. Bars in (A–C) and (E and F) indicate $\pm$SEM; Boxes in (D) represent fiber areas between the 25th and 75th percentiles; midline indicates median fiber area; bars extend to minimum and maximum area measurements. Asterisks indicate significant difference from *mdx:urtn*$^{-/-}$ ($P < 0.05$).

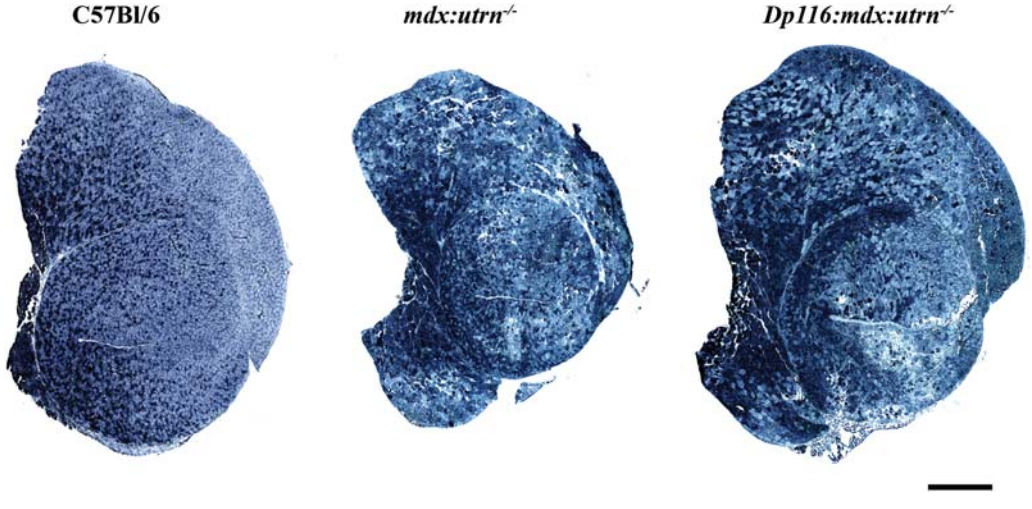

Figure 5. Expression of Dp116 does not prevent the fiber-type abnormality in *mdx:utrn*$^{-/-}$ muscles. Shown are entire cross-sections of quadriceps muscles stained with NADH. Dark staining indicates oxidative fibers while light staining indicates glycolytic fibers. Wild-type C57Bl/6 quadriceps show a mosaic pattern of oxidative and glycolytic fibers while both the *mdx:utrn*$^{-/-}$ and transgenic quadriceps show a much higher proportion of oxidative fibers as well as an increase in intermediately stained fibers. Scale bar: 1 mm.

junction in muscles of *mdx:utrn*$^{-/-}$ mice is highly fragmented, with a reduced number of synaptic folds (9,29). This could simply be a consequence of muscle degeneration, or a direct result of reduction or absence of DGC members from the neuromuscular synapse. To test this possibility, we analyzed synapses in wild-type, *mdx:utrn*$^{-/-}$ and *Dp116:mdx:utrn*$^{-/-}$ mice. We found that the Dp116 transgene had no effect in preventing synaptic fragmentation or maintaining the normal number of synaptic folds (Fig. 7). In contrast, the Δcys dystrophin mutant protein (Fig. 1A) has been reported to reduce the degree of fragmentation of the neuromuscular synapse despite lacking a functional dystroglycan-binding domain (29). Here we show

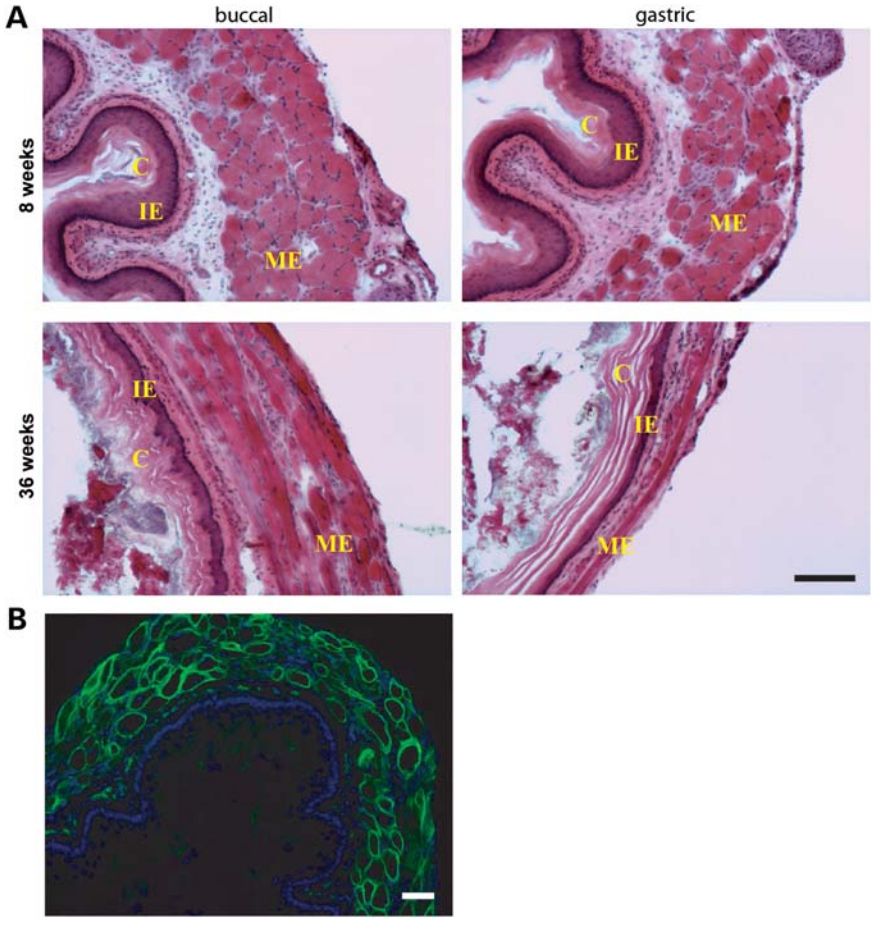

Figure 6. Magnified view of esophageal cross-sections from *Dp116:mdx:utrn*$^{-/-}$ mice. (**A**) Esophageal wall in aged (36 weeks) mice but not young (8 weeks) mice is substantially thinned overall and exhibits hyperkeratinization and exaggeration of the cornified epithelial layer (labeled 'C'). Intermediate epithelial zones (IE) are reduced or absent. The muscularis externa (ME) is stretched and diminished. Scale bar: 50 μm (five mice were analyzed). (**B**) Dp116 expression (green) in esophageal skeletal muscle. Nuclei were stained with 4′,6-diamidino-2-phenylindole (DAPI) (blue). Scale bar: 50 μm.

that restoration of the C-terminal region of dystrophin and the DGC had little effect on synapse maturation and maintenance in *mdx:utrn*$^{-/-}$ mice. These results are consistent with previous assumptions that synapse fragmentation is caused by muscle degeneration (33).

Dp116 does not confer mechanical stability to myofibers

To decipher the mechanism through which Dp116 contributes to phenotypic improvement in *mdx:utrn*$^{-/-}$ mice, we systemically injected young *mdx:utrn*$^{-/-}$ mice with a recombinant adeno-associated viral vector (rAAV6) carrying the Dp116 transgene. rAAV6 is a small, non-integrating vector that is known to efficiently transduce mature skeletal muscle (34). At 4 weeks post-injection, we observed robust and widespread Dp116 expression in multiple muscles (Fig. 8). However, treated mice failed to demonstrate any overt phenotypic improvement when compared with untreated animals and continued to display growth retardation and contractures (data not shown). Immunofluorescent analysis revealed that Dp116-positive fibers were gradually lost from skeletal muscle following the initial peak in expression at 4 weeks. By 10 weeks post-injection, Dp116 expression in skeletal muscle was severely reduced or absent, indicating that episomal rAAV6-Dp116 genomes were lost during myofiber necrosis and regeneration. In contrast, Dp116 expression was retained for up to 5 months post-injection in *mdx* muscles, which exhibit a milder dystrophy compared with *mdx:utrn*$^{-/-}$ muscles (data not shown). Thus, it is apparent that the loss of rAAV6-delivered Dp116 is dependent on the severity of dystrophic turnover, rather than any inherent instability of the construct. The loss of vector during muscle regeneration results in part from the inability of rAAV6 vectors to transduce muscle satellite cells *in vivo*, such that muscle regeneration is not accompanied by replenishment of rAAV vector genomes from the muscle stem cell pool (Arnett *et al*., manuscript in preparation). These results demonstrate that Dp116-positive fibers are not mechanically protected from dystrophic turnover and implicate a non-mechanical mechanism for Dp116-mediated rescue in transgenic *Dp116:mdx:utrn*$^{-/-}$ mice.

DISCUSSION

Several transgenic and viral vector treated mouse models have previously succeeded in ameliorating *mdx:utrn*$^{-/-}$ muscle pathology to varying degrees by expression of different

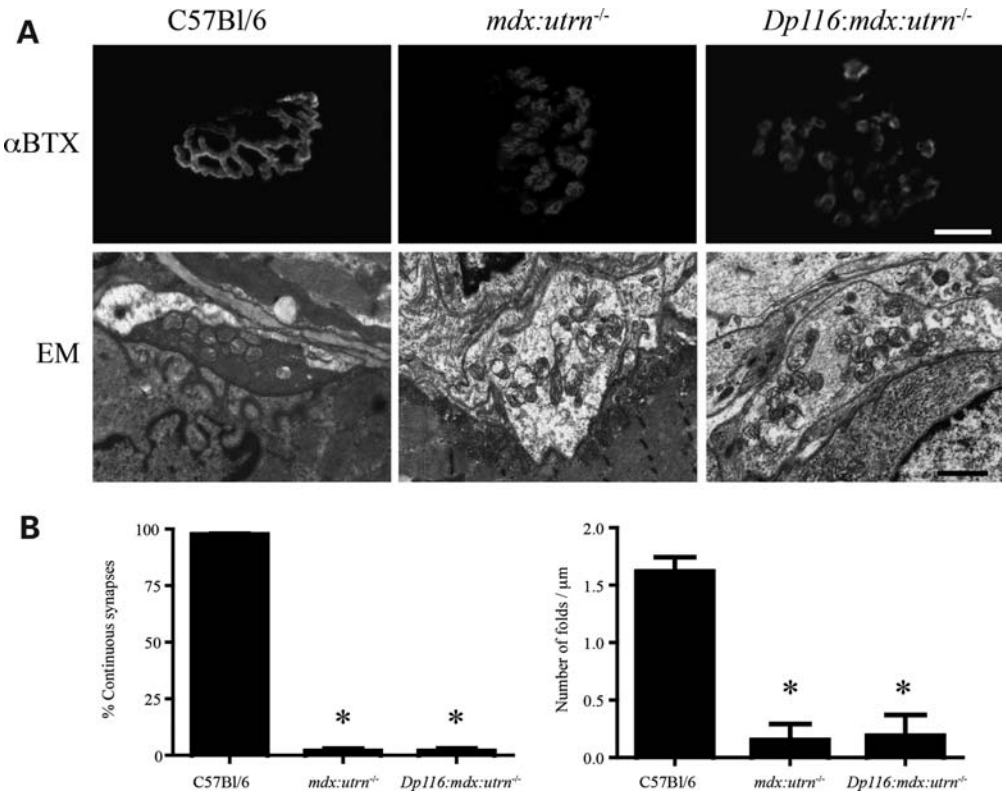

Figure 7. Dp116 has no effect on the maturation or maintenance of the neuromuscular synapse in *mdx:utrn*$^{-/-}$ mice. (**A**) The acetylcholine receptors stained with α-bungarotoxin (αBTX) are continuous in wild-type muscles, but fragmented in *mdx:utrn*$^{-/-}$ mice and *Dp116:mdx:utrn*$^{-/-}$ muscles. Electron microscopy (EM) images of the neuromuscular synapse shows a reduction in synaptic folds in *mdx:utrn*$^{-/-}$ and *Dp116:mdx:utrn*$^{-/-}$ muscles compared with wild-type muscles. (**B**) Quantitative analysis of the data presented in (A) showing that the percent of continuous synapses and the density of folds in the postsynaptic membrane are not increased by expression of Dp116 in *mdx:utrn*$^{-/-}$ mice. Bars show the mean ± S.D (*$P < 0.001$ compared with wild-type mice). Scale bar for images stained with αBTX is 15 μm and for EM images is 1 μm.

dystrophin and utrophin isoforms, as well as α7-integrin (27,29,35–38). Conversely, transgenic mice expressing the dystrophin isoform Dp71 or a dystrophin mutant with a deletion in the cysteine-rich domain (Δcys) failed to improve the phenotype of *mdx:utrn*$^{-/-}$ mice (29,39). Although Dp71 does assemble the DGC, unlike Dp116 it has an incomplete WW domain (Fig. 1A). Both the cysteine-rich region and the WW domain are essential for dystrophin binding to β-dystroglycan (40). The dystrophin–dystroglycan interaction forms the central axis of the DGC and is likely to be in dynamic equilibrium with other protein–protein interactions (17,20,41–43).

Multiple groups have proposed that perturbation of signaling pathways is an important mechanism of cell death in muscular dystrophies caused by defects in the DGC (reviewed in 22,44). These pathways could regulate a multitude of processes critical for the maintenance of healthy muscle tissue, including apoptosis, hypertrophy, regeneration and vascular blood flow. However, targeting of specific signaling pathways for potential treatment of DMD has had limited success (45,46). In fact, no specific signaling defect has yet been identified as a major factor contributing to growth retardation in dystrophin-deficient animal models, although the loss of nNOS leads to exercise-induced ischemia and fatigue (47–49). One report compared gene expression patterns of *mdx* and *mdx:utrn*$^{-/-}$ limb and extraocular muscles by DNA microarray (30). These authors hoped to identify signaling pathways responsible for the differential degree of pathology between genotypes and between muscle groups that would manifest as alterations in levels of gene expression. Interestingly, the most significantly upregulated genes in *mdx:utrn*$^{-/-}$ muscles were not known signaling molecules but were proteins associated with the slow muscle fiber phenotype. The authors proposed that this expression pattern and fiber-type composition contributes to the severe *mdx:utrn*$^{-/-}$ phenotype. It was previously demonstrated that *mdx:utrn*$^{-/-}$ muscles have a preponderance of slow oxidative fibers, as well as a highly fragmented pattern of acetylcholine receptors at the post-synaptic membrane (9,29). Both of these abnormalities were partially corrected by the Δcys dystrophin mutant, which does not prevent dystrophy nor restore the DGC but does have full N-terminal and central actin-binding domains (29). We found no significant change in fiber-type composition (Fig. 5) or the structure of the post-synaptic membrane in muscles of mice expressing Dp116 (Fig. 7), despite the dramatic improvement in muscle function. This result indicates that these abnormalities are not likely to be causative of the severe phenotype of *mdx:utrn*$^{-/-}$ but may instead be a consequence of, or a compensatory response to, the cycles of myofiber degeneration and regeneration (50,51). It is of interest that neuromuscular junctions associated with a DGC unable to bind actin lack junctional folds despite the relatively normal muscle mass (Figs 2 and 7).

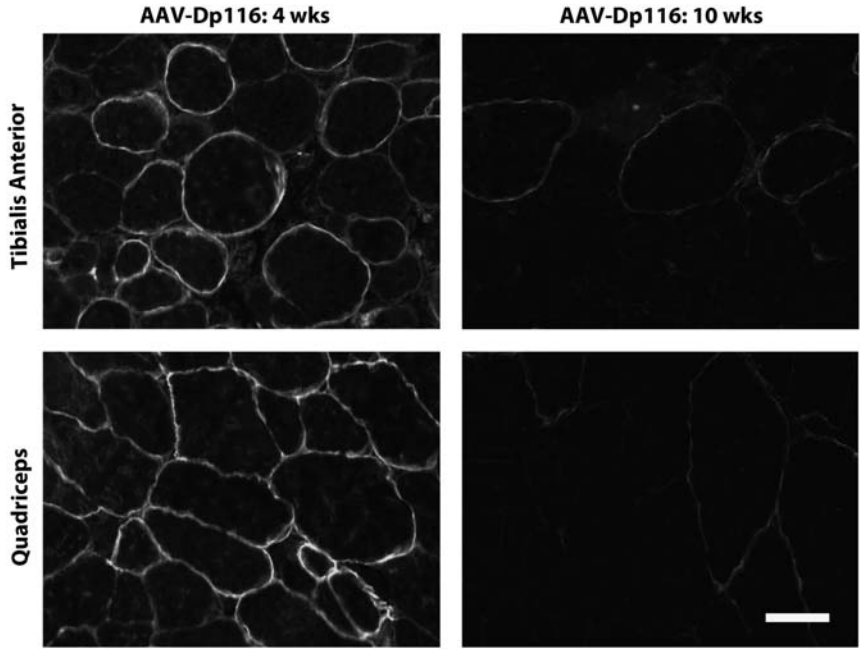

Figure 8. rAAV6-delivered Dp116 does not protect myofibers from dystrophic turnover. *mdx:utrn*$^{-/-}$ mice were treated with rAAV6-Dp116 at 2 weeks of age. Quadriceps (bottom) and TA (top) were collected and analyzed for Dp116 expression via immunofluorescent staining. At 4 weeks post-injection (left), robust expression of Dp116 is observed. In contrast, Dp116 expression is nearly absent at 10 weeks post-injection (right).

Most studies of dystrophin structure–function have generated evidence favoring the importance of a mechanical role in preventing dystrophic injury. Dystrophin mutations that perturb either the actin-binding or the dystroglycan-binding domains of dystrophin compromise the ability of the protein to prevent dystrophic damage to the muscle, even if all functional domains are present via simultaneous expression of two different dystrophin mutants (23–25,39,52,53). These results emphasize the importance of maintaining the mechanical link between the extracellular matrix and the actin cytoskeleton. We reported that systemic delivery of a micro-dystrophin gene using a viral vector led to increased muscle mass and extended the lifespan of *mdx:utrn*$^{-/-}$ mice (27). In that case, expression of a truncated dystrophin (similar in size to Dp116 but containing a functional N-terminal actin-binding domain) increased myofiber size and specific force while reducing signs of dystrophic injury; none of these parameters was altered by Dp116 expression. Surprisingly, expression of Dp116 increased muscle mass and extended lifespan to a similar degree as the micro-dystrophin despite a lack of protection from dystrophy. Furthermore, the rapid loss of rAAV6-delivered Dp116 in *mdx:utrn*$^{-/-}$ muscle clearly demonstrates that Dp116 does not protect myofibers from dystrophic degeneration (Fig. 8). The high degree of central nucleation and the histopathological appearance of *Dp116:mdx:utrn*$^{-/-}$ muscle (Fig. 4) lend further support to this conclusion. Recombinant AAV6 is known to persist within the cell in an episomal state, and cellular turnover has been associated with the loss of vector genomes *in vivo* (54). As non-integrated structures, episomal vector genomes would be lost during fiber necrosis, and degenerated fibers subsequently replaced by newly generated, Dp116-negative myofibers in non-transgenic animals. In contrast, muscle regeneration in Dp116 transgenic *mdx:utrn*$^{-/-}$ mice results in maintenance of Dp116 expression in regenerated myofibers, which leads to a significant phenotypic amelioration.

We interpret the above data as evidence for the lack of a mechanical function of Dp116, and that the mechanical function of full-length dystrophin primarily serves to protect against dystrophic injury. We cannot exclude the possibility that Dp116 contributes to stability of the sarcolemma through alternate interactions between the DGC and the cytoskeleton. It is clear that the network of cytoskeletal proteins associated with costameres is extensive, and dystrophin has been shown recently to interact with microtubules and intermediate filaments, interactions that may well occur with Dp116 (55,56). This may explain the modest improvement seen in resistance to contraction-induced injury, as restoration of a normal costameric lattice may improve lateral force transmission to adjacent myofibers (16). However, our results with both dystrophin-deficient and dystrophin/utrophin double-knockout mice demonstrate that any such interactions made by the Dp116/DGC complex are ultimately incapable of functionally substituting for the direct actin-binding properties of dystrophin or utrophin. The seemingly paradoxical improvement in muscle mass and function implicates a distinct function of dystrophin and the DGC that has not been previously described.

One cellular mechanism that is likely to be defective in *mdx:utrn*$^{-/-}$ mice is regeneration. Until late in their lifespan, *mdx* mice show efficient regeneration of skeletal muscle that maintains muscle mass despite ongoing myofiber necrosis (8,57). Regeneration of skeletal muscle is primarily dependent on satellite cells, the resident stem cell population (58). Maintenance of regeneration has been proposed to explain the relatively mild phenotype of mice in which dystroglycan was

disrupted specifically in skeletal muscle. These mice were generated using a muscle creatine kinase promoter driven Cre-loxP system to delete the dystroglycan gene in skeletal myofibers (59). This cross resulted in the complete disruption of the DGC in mature myofibers, but not in satellite cells or regenerating fibers. The authors concluded that expression of dystroglycan in muscle precursor cells is critical for continued regeneration, which efficiently compensated for muscle damage in their mice.

Our study is the first demonstration of an important functional role for restoration of the DGC without a concomitant link to the actin cytoskeleton by dystrophin or utrophin. When contrasted with the failure of Dp71 to produce a similar improvement in phenotype, our data suggest that a strong interaction between dystrophin and dystroglycan may be necessary for regulation of vital functions of the DGC that is separate from the linkage between the actin cytoskeleton and sarcolemma created by full-length dystrophin. We suggest that this function may be a signaling mechanism that regulates muscle growth and/or regeneration.

MATERIALS AND METHODS

Animals

To generate *Dp116:mdx:utrn*$^{-/-}$ mice, male *Dp116:mdx*^{4cv} mice hemizygous for the *Dp116* transgene were mated with *mdx:utrn*$^{-/+}$ females (9). The starting *Dp116:mdx*^{4cv} transgenic mice had been backcrossed against the *mdx*^{4cv} strain for more than six generations and were described previously (25). The *Dp116*-positive *mdx:utrn*$^{-/+}$ male progeny of this first cross was mated for a second generation with *mdx:utrn*$^{-/+}$ females. The second cross produced six possible genotypes: *mdx*, *mdx:utrn*$^{-/+}$ and *mdx:utrn*$^{-/-}$, each either positive or negative for the *Dp116* transgene. This breeding scheme was carried out independently with two different lines of *Dp116* transgenic mice (2197 and 2354). All mice were genotyped by polymerase chain reaction at weaning age for both the utrophin mutation (60) and the *Dp116* transgene (25). Selected mice were genotyped for the *mdx* mutation by an amplification-resistant mutation system assay (61). As expected, all mice tested were positive for the *mdx* mutation. Mice were weighed weekly after weaning and assignment of genotype. Both standard *mdx* and *mdx*^{4cv} animals were used as controls for histological and physiological experiments. No significant differences were noted between the two genotypes so the data were combined and referred to as simply *mdx* in all figures. All experimental protocols were approved by the Institutional Animal Care and Use Committee of the University of Washington.

Measurement of serum creatine kinase levels

Blood was drawn from 8- to 10-week-old live mice via retro-orbital bleeds. The whole blood was immediately centrifuged and the serum collected and stored at 4°C. Measurement of the creatine kinase level was performed within 24 h of collection using the Stanbio CK, Liqui-UV kit (Stanbio Laboratory). For each measurement, individual samples were run in triplicate and compared with control normal and abnormal serum (Stanbio Ser-T-Fy I and Stanbio Ser-T-Fy II) to verify consistent results.

rAAV vector production and delivery

Flag-tagged Dp116 was inserted into an rAAV6 expression plasmid containing the cytomegalovirus immediate early enhancer + promoter, flanking inverted terminal repeats, and an SV40 polyA sequence. All vectors were prepared as described previously, using a two-plasmid co-transfection method into human embryonic kidney-293 cells followed by heparin-column purification (34). Vector titer was evaluated via southern analysis. Mice ($n = 5$) were injected intravenously with 10^{12} vector genomes (diluted in 200 μl isotonic saline) at ~2 weeks of age. An additional cohort of *mdx* ($n = 8$) and *mdx:utrn*$^{-/-}$ ($n = 3$) animals received IM injections (under isofluorane anesthesia) at a dose of 10^{10} vector genomes in 25 μl isotonic saline.

Immunofluorescence

Selected tissues were dissected, embedded in OCT (Sakura Finetek USA) and frozen in liquid nitrogen-cooled isopentane. Cryosections of 7–10 μm thickness were blocked in KPBS (20 mM potassium phosphate pH 7.4, 150 mM sodium chloride) containing 0.3 mg/ml bovine serum albumin (BSA) and 1% Tween 20. The blocked sections were incubated with primary antibodies diluted in KPBS containing 0.2% gelatin (KPBS-G) and 2% normal goat serum. Rabbit polyclonal antibodies were used to label Flag (Sigma), dystrophin NH_2-terminus (53) and utrophin A (S. Froehner, unpublished data). After several washes with KBPS-G, the sections were incubated with goat anti-rabbit Alexafluor 488 (Molecular Probes). Immunostained slides were washed repeatedly with KBPS-G and mounted with Vectashield (Vector Laboratories). All photomicrographs were obtained with a Spot II CCD camera (Diagnostic Instruments, Inc.) and Spot Advanced software connected to a Nikon Eclipse E1000 using a ×20 Plan-Apochromat objective (numerical aperture = 0.75). Images for all the sections probed with a given antibody were acquired under identical exposure conditions.

Histological analysis and quantitative measurements of muscle fibers

Muscles were dissected, embedded in OCT (Sakura Finetek USA) and frozen in liquid nitrogen-cooled isopentane. Cryosections of 10 μm thickness were briefly fixed in methanol and stained with Gill's hematoxylin and eosin-phyloxine. The sections were washed, dehydrated and cleared in xylene before mounting with Permount. NADH staining was performed by incubating unfixed sections in 0.2 M Tris pH 7.4, 1.5 mM β-NADH reduced form disodium salt (Sigma) and 1.5 mM nitro-blue tetrazolium (Sigma) at 37°C for 30 min. The stained sections were washed for 2 min each in 30, 60, 90, 60 and 30% acetone and mounted in Vectashield (Vector Laboratories). Photomicrographs were obtained with a QICAM Fast cooled digital CCD camera and QCapture Pro software (QImaging) connected to a Nikon Eclipse E1000 microscope using a ×20 Plan-Apochromat objective

(numerical aperture = 0.75). Images of entire muscle cross-sections were obtained using SyncroscanRT software (Syncroscopy). Quantitative analysis of images was performed using ImageJ 1.38x software (National Institute of Health, USA). Average cross-sectional area of muscle fibers was determined by random measurement of ~500 fibers per mouse. Fiber density was calculated independently through random selection of four 0.13 mm^2 fields per muscle cross-section. These fields were used to measure both fiber density and the percentage of myofibers with centrally located nuclei. Statistical analysis was performed via analysis of variation (ANOVA) followed by a Tukey post-test using Graphpad Prism software.

Electron microscopy

Small (~1 mm^3) regions of diaphragm muscles from 3-month-old wild-type, *mdx:utrn* −/− and *mdx:utrn* −/− mice expressing the Dp 116 transgene were fixed in half strength Karnovskys fixative for at least 24 h at 4°C. Fixed muscles were washed in 1× phosphate buffer (pH 7.1), post-fixed in 1% (*w/v*) aqueous osmium tetroxide containing 1.5% (*w/v*) potassium ferrocyanide (62), stained en bloc with uranyl acetate, dehydrated through acetone into Epon resin, embedded and polymerized at 60°C for 24 h. Ultrathin sections were cut at ~ 80 nm, stained with Reynolds lead citrate (63), viewed and photographed with a Hitachi H600 transmission electron microscope (Tokyo, Japan). Synaptic folds were quantified using Image J (NIH) and compared using a one-way ANOVA with a Tukey post-test.

Neuromuscular synapse immunostaining

For wholemount preparations, skeletal muscle fibers were fixed for 2 h in 2% paraformaldehyde at 4°C. Immediately following fixation, individual muscle fibers were teased apart using a fine needle. The fibers were then incubated 0.1 M glycine for 30 min, blocked in blocking solution (1% BSA, 0.05% Triton X-100 in 1× PBS) for 1 h and stained with TRITC-conjugated α-bungarotoxin (αBTX; 1:500; Molecular Probes) for 1 h. The fibers were washed three times in blocking solution after staining and mounted on slides with antifade mounting media containing 4′,6-diamidino-2-phenylindole (Vector Labs). Synapses were viewed and photographed using a Leica SL confocal microscope. Synapses were classified as continuous if they presented with three or less continuous regions of AChR clustering and discontinuous if they presented with more than three regions of AChR clustering. Approximately 600 synapses from $n = 4$ mice were analyzed and compared using a one-way ANOVA with a Tukey post-test.

Functional analyses

Force generation and susceptibility to contraction-induced injury was evaluated using a procedure previously developed by our laboratory (27). Briefly, male mice from 8 to 10 weeks of age were anesthetized with 2,2,2-tribromoethanol (Sigma) for *in situ* analysis of TA. Maximal force generation was evaluated at optimal muscle fiber length. Contractile performance was measured during a series of progressively increasing lengthening contractions stimulated at 10 s intervals. Following contractile evaluation, the TA was removed and weighed to calculate specific force. One-way ANOVA and Tukey post-test analyses were performed using GraphPad Prism software.

SUPPLEMENTARY MATERIAL

Supplementary Material is available at *HMG* online.

ACKNOWLEDGEMENTS

We are grateful to Greg Martin at the Keck Imaging Center University of Washington for help with confocal microscopy, and Judith Bousman and Bobby Schneider for help with electron microscopy. Thanks to Stanley Froehner and Marvin Adams for kindly supplying the antibody to utrophin-A, James Allen, Eric Finn and Caitlin Doremus for assistance with vector production, Miki Haraguchi for technical assistance, Paul Gregorevic and Michael Blankinship for advice and help with mouse breeding and genotyping.

Conflict of Interest statement. None declared.

FUNDING

This work was supported by the National Institutes of Health (RO1AR44533 to J.S.C., F30NS068005 to A.L.H.A.), by the Medical Scientist Training Program (to L.M.J. and A.L.H.A.), a Poncin Scholarship Fund (to L.M.J.), an Achievement Rewards for College Scientists (to L.M.J. and A.L.H.A.), a CJ Martin Post-Doctoral Fellowship from the National Health and Medical Research Council of Australia (372212 to G.B.B.) and a Development Grant from the Muscular Dystrophy Association (USA) (to G.B.B.).

REFERENCES

1. Emery, A.E. and Muntoni, F. (2003) *Duchenne Muscular Dystrophy*. Oxford University Press, Oxford.
2. Bulfield, G., Siller, W.G., Wight, P.A. and Moore, K.J. (1984) X chromosome-linked muscular dystrophy (*mdx*) in the mouse. *Proc. Natl Acad. Sci. USA*, **81**, 1189–1192.
3. Carnwath, J.W. and Shotton, D.M. (1987) Muscular dystrophy in the mdx mouse: histopathology of the soleus and extensor digitorum longus muscles. *J. Neurol. Sci.*, **80**, 39–54.
4. Coulton, G.R., Morgan, J.E., Partridge, T.A. and Sloper, J.C. (1988) The mdx mouse skeletal muscle myopathy: I. A histological, morphometric and biochemical investigation. *Neuropathol. Appl. Neurobiol.*, **14**, 53–70.
5. Chamberlain, J.S. (2010) Duchenne muscular dystrophy models show their age. *Cell*, **143**, 1040–1042.
6. Coulton, G.R., Curtin, N.A., Morgan, J.E. and Partridge, T.A. (1988) The mdx mouse skeletal muscle myopathy: II. Contractile properties. *Neuropathol. Appl. Neurobiol.*, **14**, 299–314.
7. Lefaucheur, J.P., Pastoret, C. and Sebille, A. (1995) Phenotype of dystrophinopathy in old mdx mice. *Anat. Rec.*, **242**, 70–76.
8. Chamberlain, J.S., Metzger, J., Reyes, M., Townsend, D. and Faulkner, J.A. (2007) Dystrophin-deficient *mdx* mice display a reduced life span and are susceptible to spontaneous rhabdomyosarcoma. *FASEB J.*, **21**, 2195–2204.
9. Grady, R.M., Teng, H., Nichol, M.C., Cunningham, J.C., Wilkinson, R.S. and Sanes, J.R. (1997) Skeletal and cardiac myopathies in mice lacking utrophin and dystrophin: a model for Duchenne muscular dystrophy. *Cell*, **90**, 729–738.

10. Deconinck, A.E., Rafael, J.A., Skinner, J.A., Brown, S.C., Potter, A.C., Metzinger, L., Watt, D.J., Dickson, J.G., Tinsley, J.M. and Davies, K.E. (1997) Utrophin-dystrophin-deficient mice as a model for Duchenne muscular dystrophy. *Cell*, **90**, 717–727.
11. Tinsley, J., Deconinck, N., Fisher, R., Kahn, D., Phelps, S., Gillis, J.M. and Davies, K. (1998) Expression of full-length utrophin prevents muscular dystrophy in mdx mice. *Nat. Med.*, **4**, 1441–1444.
12. Abmayr, S. and Chamberlain, J. (2006) Winder, S.J. (ed.), *Molecular Mechanisms of Muscular Dystrophies*. Landes Biosciences, Georgetown, pp. 14–34.
13. Ervasti, J.M. and Campbell, K.P. (1993) A role for the dystrophin-glycoprotein complex as a transmembrane linker between laminin and actin. *J. Cell Biol.*, **122**, 809–823.
14. Rybakova, I.N., Patel, J.R. and Ervasti, J.M. (2000) The dystrophin complex forms a mechanically strong link between the sarcolemma and costameric actin. *J. Cell Biol.*, **150**, 1209–1214.
15. Petrof, B.J., Shrager, J.B., Stedman, H.H., Kelly, A.M. and Sweeney, H.L. (1993) Dystrophin protects the sarcolemma from stresses developed during muscle contraction. *Proc. Natl Acad. Sci. USA*, **90**, 3710–3714.
16. Ramaswamy, K.S., Palmer, M.L., van der Meulen, J.H., Renoux, A., Kostrominova, T.Y., Michele, D.E. and Faulkner, J.A. (2011) Lateral transmission of force is impaired in skeletal muscles of dystrophic mice and very old rats. *J. Physiol.*, **589**, 1195–1208.
17. Yang, B., Jung, D., Motto, D., Meyer, J., Koretzky, G. and Campbell, K.P. (1995) SH3 domain-mediated interaction of dystroglycan and Grb2. *J. Biol. Chem.*, **270**, 11711–11714.
18. Brenman, J.E., Chao, D.S., Xia, H., Aldape, K. and Bredt, D.S. (1995) Nitric oxide synthase complexed with dystrophin and absent from skeletal muscle sarcolemma in Duchenne muscular dystrophy. *Cell*, **82**, 743–752.
19. Sotgia, F., Lee, J.K., Das, K., Bedford, M., Petrucci, T.C., Macioce, P., Sargiacomo, M., Bricarelli, F.D., Minetti, C., Sudol, M. *et al.* (2000) Caveolin-3 directly interacts with the C-terminal tail of beta -dystroglycan. Identification of a central WW-like domain within caveolin family members. *J. Biol. Chem.*, **275**, 38048–38058.
20. Sotgia, F., Lee, H., Bedford, M.T., Petrucci, T., Sudol, M. and Lisanti, M.P. (2001) Tyrosine phosphorylation of beta-dystroglycan at its WW domain binding motif, PPxY, recruits SH2 domain containing proteins. *Biochemistry*, **40**, 14585–14592.
21. Spence, H.J., Dhillon, A.S., James, M. and Winder, S.J. (2004) Dystroglycan, a scaffold for the ERK-MAP kinase cascade. *EMBO Rep.*, **5**, 484–489.
22. Rando, T.A. (2001) The dystrophin-glycoprotein complex, cellular signaling, and the regulation of cell survival in the muscular dystrophies. *Muscle Nerve*, **24**, 1575–1594.
23. Cox, G.A., Sunada, Y., Campbell, K.P. and Chamberlain, J.S. (1994) Dp71 can restore the dystrophin-associated glycoprotein complex in muscle but fails to prevent dystrophy. *Nat. Genet.*, **8**, 333–339.
24. Greenberg, D.S., Sunada, Y., Campbell, K.P., Yaffe, D. and Nudel, U. (1994) Exogenous Dp71 restores the levels of dystrophin associated proteins but does not alleviate muscle damage in *mdx* mice. *Nat. Genet.*, **8**, 340–344.
25. Judge, L.M., Haraguchi, M. and Chamberlain, J.S. (2006) Dissecting the signaling and mechanical functions of the dystrophin-glycoprotein complex. *J. Cell Sci.*, **119**, 1537–1546.
26. Imamura, M., Araishi, K., Noguchi, S. and Ozawa, E. (2000) A sarcoglycan-dystroglycan complex anchors Dp116 and utrophin in the peripheral nervous system. *Hum. Mol. Genet.*, **9**, 3091–3100.
27. Gregorevic, P., Allen, J.M., Minami, E., Blankinship, M.J., Haraguchi, M., Meuse, L., Finn, E., Adams, M.E., Froehner, S.C., Murry, C.E. *et al.* (2006) rAAV6-microdystrophin preserves muscle function and extends lifespan in severely dystrophic mice. *Nat. Med.*, **12**, 787–789.
28. Dellorusso, C., Crawford, R.W., Chamberlain, J.S. and Brooks, S.V. (2001) Tibialis anterior muscles in mdx mice are highly susceptible to contraction-induced injury. *J. Muscle Res. Cell Motil.*, **22**, 467–475.
29. Rafael, J.A., Townsend, E.R., Squire, S.E., Potter, A.C., Chamberlain, J.S. and Davies, K.E. (2000) Dystrophin and utrophin influence fiber type composition and post-synaptic membrane structure. *Hum. Mol. Genet.*, **9**, 1357–1367.
30. Baker, P.E., Kearney, J.A., Gong, B., Merriam, A.P., Kuhn, D.E., Porter, J.D. and Rafael-Fortney, J.A. (2006) Analysis of gene expression differences between utrophin/dystrophin-deficient vs mdx skeletal muscles reveals a specific upregulation of slow muscle genes in limb muscles. *Neurogenetics*, **7**, 81–91.
31. Banks, G.B., Fuhrer, C., Adams, M.E. and Froehner, S.C. (2003) The postsynaptic submembrane machinery at the neuromuscular junction: requirement for rapsyn and the utrophin/dystrophin-associated complex. *J. Neurocytol.*, **32**, 709–726.
32. Grady, R.M., Zhou, H., Cunningham, J.M., Henry, M.D., Campbell, K.P. and Sanes, J.R. (2000) Maturation and maintenance of the neuromuscular synapse: genetic evidence for roles of the dystrophin-glycoprotein complex. *Neuron*, **25**, 279–293.
33. Lyons, P.R. and Slater, C.R. (1991) Structure and function of the neuromuscular junction in young adult mdx mice. *J. Neurocytol.*, **20**, 969–981.
34. Gregorevic, P., Blankinship, M.J., Allen, J.M., Crawford, R.W., Meuse, L., Miller, D.G., Russell, D.W. and Chamberlain, J.S. (2004) Systemic delivery of genes to striated muscles using adeno-associated viral vectors. *Nat. Med.*, **10**, 828–834.
35. Gaedigk, R., Law, D.J., Fitzgerald-Gustafson, K.M., McNulty, S.G., Nsumu, N.N., Modrcin, A.C., Rinaldi, R.J., Pinson, D., Fowler, S.C., Bilgen, M. *et al.* (2006) Improvement in survival and muscle function in an mdx/utrn(−/−) double mutant mouse using a human retinal dystrophin transgene. *Neuromuscul. Disord.*, **16**, 192–203.
36. Burkin, D.J., Wallace, G.Q., Nicol, K.J., Kaufman, D.J. and Kaufman, S.J. (2001) Enhanced expression of the alpha 7 beta 1 integrin reduces muscular dystrophy and restores viability in dystrophic mice. *J. Cell Biol.*, **152**, 1207–1218.
37. Rafael, J.A., Tinsley, J.M., Potter, A.C., Deconinck, A.E. and Davies, K.E. (1998) Skeletal muscle-specific expression of a utrophin transgene rescues utrophin-dystrophin deficient mice. *Nat. Genet.*, **19**, 79–82.
38. Odom, G.L., Gregorevic, P., Allen, J.M., Finn, E. and Chamberlain, J.S. (2008) Microutrophin delivery through rAAV6 increases lifespan and improves muscle function in dystrophic dystrophin/utrophin-deficient mice. *Mol. Ther.*, **16**, 1539–1545.
39. Gardner, K.L., Kearney, J.A., Edwards, J.D. and Rafael-Fortney, J.A. (2005) Restoration of all dystrophin protein interactions by functional domains in trans does not rescue dystrophy. *Gene Ther.*, **13**, 744–751.
40. Huang, X., Poy, F., Zhang, R., Joachimiak, A., Sudol, M. and Eck, M.J. (2000) Structure of a WW domain containing fragment of dystrophin in complex with beta-dystroglycan. *Nat. Struct. Biol.*, **7**, 634–638.
41. Ilsley, J.L., Sudol, M. and Winder, S.J. (2002) The WW domain: linking cell signalling to the membrane cytoskeleton. *Cell Signal.*, **14**, 183–189.
42. James, M., Nuttall, A., Ilsley, J.L., Ottersbach, K., Tinsley, J.M., Sudol, M. and Winder, S.J. (2000) Adhesion-dependent tyrosine phosphorylation of (beta)-dystroglycan regulates its interaction with utrophin. *J. Cell Sci.*, **113**, 1717–1726.
43. Galbiati, F., Volonte, D., Chu, J.B., Li, M., Fine, S.W., Fu, M., Bermudez, J., Pedemonte, M., Weidenheim, K.M., Pestell, R.G. *et al.* (2000) Transgenic overexpression of caveolin-3 in skeletal muscle fibers induces a Duchenne-like muscular dystrophy phenotype. *Proc. Natl Acad. Sci. USA*, **97**, 9689–9694.
44. Winder, S.J. (2005) Winder, S.J. (ed.) *Molecular Mechanisms of Muscular Dystrophies*. Landes Biosciences, Georgetown, pp. 198–210.
45. Wehling, M., Spencer, M.J. and Tidball, J.G. (2001) A nitric oxide synthase transgene ameliorates muscular dystrophy in mdx mice. *J. Cell Biol.*, **155**, 123–131.
46. Kolodziejczyk, S.M., Walsh, G.S., Balazsi, K., Seale, P., Sandoz, J., Hierlihy, A.M., Rudnicki, M.A., Chamberlain, J.S., Miller, F.D. and Megeney, L.A. (2001) Activation of JNK1 contributes to dystrophic muscle pathogenesis. *Curr. Biol.*, **11**, 1278–1282.
47. Crosbie, R.H., Straub, V., Yun, H.Y., Lee, J.C., Rafael, J.A., Chamberlain, J.S., Dawson, V.L., Dawson, T.M. and Campbell, K.P. (1998) mdx muscle pathology is independent of nNOS perturbation. *Hum. Mol. Genet.*, **7**, 823–829.
48. Kobayashi, Y.M., Rader, E.P., Crawford, R.W., Iyengar, N.K., Thedens, D.R., Faulkner, J.A., Parikh, S.V., Weiss, R.M., Chamberlain, J.S., Moore, S.A. *et al.* (2008) Sarcolemma-localized nNOS is required to maintain activity after mild exercise. *Nature*, **456**, 511–515.
49. Lai, Y., Thomas, G.D., Yue, Y., Yang, H.T., Li, D., Long, C., Judge, L., Bostick, B., Chamberlain, J.S., Terjung, R.L. *et al.* (2009) Dystrophins carrying spectrin-like repeats 16 and 17 anchor nNOS to the sarcolemma and enhance exercise performance in a mouse model of muscular dystrophy. *J. Clin. Invest.*, **119**, 624–635.

50. Handschin, C., Kobayashi, Y.M., Chin, S., Seale, P., Campbell, K.P. and Spiegelman, B.M. (2007) PGC-1alpha regulates the neuromuscular junction program and ameliorates Duchenne muscular dystrophy. *Genes Dev.*, **21**, 770–783.
51. Chakkalakal, J.V., Harrison, M.A., Carbonetto, S., Chin, E., Michel, R.N. and Jasmin, B.J. (2004) Stimulation of calcineurin signaling attenuates the dystrophic pathology in mdx mice. *Hum. Mol. Genet.*, **13**, 379–388.
52. Banks, G.B., Gregorevic, P., Allen, J.M., Finn, E.E. and Chamberlain, J.S. (2007) Functional capacity of dystrophins carrying deletions in the N-terminal actin-binding domain. *Hum. Mol. Genet.*, **16**, 2105–2113.
53. Rafael, J.A., Cox, G.A., Corrado, K., Jung, D., Campbell, K.P. and Chamberlain, J.S. (1996) Forced expression of dystrophin deletion constructs reveals structure-function correlations. *J. Cell Biol.*, **134**, 93–102.
54. Nakai, H., Yant, S.R., Storm, T.A., Fuess, S., Meuse, L. and Kay, M.A. (2001) Extrachromosomal recombinant adeno-associated virus vector genomes are primarily responsible for stable liver transduction in vivo. *J. Virol.*, **75**, 6969–6976.
55. Ervasti, J.M. (2003) Costameres: the Achilles' heel of Herculean muscle. *J. Biol. Chem.*, **278**, 13591–13594.
56. Prins, K.W., Humston, J.L., Mehta, A., Tate, V., Ralston, E. and Ervasti, J.M. (2009) Dystrophin is a microtubule-associated protein. *J. Cell Biol.*, **186**, 363–369.
57. Lynch, G.S., Hinkle, R.T., Chamberlain, J.S., Brooks, S.V. and Faulkner, J.A. (2001) Force and power output of fast and slow skeletal muscles from mdx mice 6–28 months old. *J. Physiol.*, **535**, 591–600.
58. Collins, C.A., Olsen, I., Zammit, P.S., Heslop, L., Petrie, A., Partridge, T.A. and Morgan, J.E. (2005) Stem cell function, self-renewal, and behavioral heterogeneity of cells from the adult muscle satellite cell niche. *Cell*, **122**, 289–301.
59. Cohn, R.D., Henry, M.D., Michele, D.E., Barresi, R., Saito, F., Moore, S.A., Flanagan, J.D., Skwarchuk, M.W., Robbins, M.E., Mendell, J.R. *et al.* (2002) Disruption of DAG1 in differentiated skeletal muscle reveals a role for dystroglycan in muscle regeneration. *Cell*, **110**, 639–648.
60. Grady, R.M., Merlie, J.P. and Sanes, J.R. (1997) Subtle neuromuscular defects in utrophin-deficient mice. *J. Cell Biol.*, **136**, 871–882.
61. Amalfitano, A. and Chamberlain, J.S. (1996) The mdx-amplification-resistant mutation system assay, a simple and rapid polymerase chain reaction-based detection of the mdx allele. *Muscle Nerve*, **19**, 1549–1553.
62. Kopriwa, B.M. (1984) Block-staining tissues with potassium ferrocyanide-reduced osmium tetroxide and lead aspartate for electron microscopic radioautography. *J. Histol. Cytochem.*, **32**, 552–554.
63. Reynolds, E.S. (1963) The use of lead citrate at high pH as an electron-opaque stain in electron microscopy. *J. Cell Biol.*, **17**, 208–212.